Optics Communications 323 (2014) 44–48

Contents lists available at ScienceDirect

Optics Communications

journal homepage: www.elsevier.com/locate/optcom

The sensing characteristics of plasmonic waveguide with a single defect

Tiesheng Wu, Yumin Liu *, Zhongyuan Yu, Yiwei Peng, Changgan Shu, Huifang He

State Key Laboratory of Information Photonics and Optical Communications, Beijing University of Posts and Telecommunications, Beijing 100876, China

ARTICLE INFO

Article history:
Received 8 January 2014
Received in revised form
26 February 2014
Accepted 28 February 2014
Available online 13 March 2014

Keywords:
Surface plasmon polaritons
Sensor
Refractive index
Temperature
Finite element method

ABSTRACT

A novel two-dimensional nanoscale structure for sensing which consists of a metal–insulator–metal (MIM) waveguide with a defect, is designed and numerically simulated by using the finite element method (FEM). Both of the refractive index sensing characteristics and the temperature sensing characteristics of the structure are analyzed systematically by investigating the transmission spectrum. The numerically simulated results show that the dip positions of the transmission spectrum have linear relationships with the refractive index of the material under sensing and the ambient temperature, respectively. Based on the relationships, the refractive index of the material under sensing or the ambient temperature can be obtained from the dip wavelength shift detection. When the width and the height of the defect are set to be 50 nm, 300 nm, respectively, the refractive index sensitivity can be obtained as high as 1736 nm RIU^{-1} and the temperature sensitivity is about 0.51 nm/°C with a FOM of 9.79. This work has a certain significance for designing nanoscale refractive index sensors and temperature sensors.

1. Introduction

Surface plasmon polaritons (SPPs) are the electromagnetic surface waves that travel along the interface between metal and dielectric with an exponentially decay to the both sides. SPPs have been considered as energy and information carriers in nanoscale optics for their ability of overcoming diffraction limit of light in conventional optics [1–4]. Surface plasmons have been widely studied over the last decades for sensing applications. Both propagating surface plasmon polaritons (SPPs) and localized surface resonances (LSPRs) exhibit very interesting properties for sensing applications due to their high degree of tenability and their susceptibility to the dielectric properties of the surrounding environment [5–14]. SPPs sensors have been investigated and studied based on various ideas such as SPPs resonance of nanoparticles and enhanced transmission through nanohole arrays [15–24]. SPPs sensors not only have the ability to attain high integration because of SPPs beyond the diffraction limit of light, but also have high sensing sensitivity. As for LSPRs sensors, they are simple, cost-effective and suitable for measuring local refractive index changes caused by the adsorption of target molecules [25–27]. However, the figure of merit (FOM), which is defined as the ratio of wavelength sensitivity to the bandwidth of resonance [a full width at half-maximum (FWHM)] [19], of LSPRs sensors are generally 1–2 orders of magnitude smaller than SPPs sensors. Owing to strong radiative damping, the LSPRs of metal nanostructures generally exhibit broad resonance peaks, which result in small FOM values and in turn limit the performances of LSPRs sensors [25].

In this paper, a SPPs sensor based on metal–insulator–metal (MIM) waveguide with a defect is proposed. We not only investigate its refractive index sensing characteristics, but also investigate its temperature sensing characteristics. The SPPs sensor performance is simulated numerically by the finite element method (FEM) with scattering boundary conditions. In the simulation, we use commercial software COMSOL Multiphysics 4.3a.

2. Theory model

Our proposed two-dimensional (2D) structure is shown in Fig. 1. The structure of the SPPs sensor is composed of a metal–insulator–metal (MIM) waveguide with a triangle defect which is considered invariant along y direction. The purple and white areas are silver and the material which need to be detected, respectively. From Fig. 1 we can see that the material (liquid or gas) under sensing is filled in the slit and the defect. d is the width of the slit. The width and the height of the defect are w and h, respectively. As is well known, the dispersion of the fundamental TM mode in a

* Corresponding author.
E-mail address: microliuyumin@hotmail.com (Y. Liu).

http://dx.doi.org/10.1016/j.optcom.2014.02.067
0030-4018/

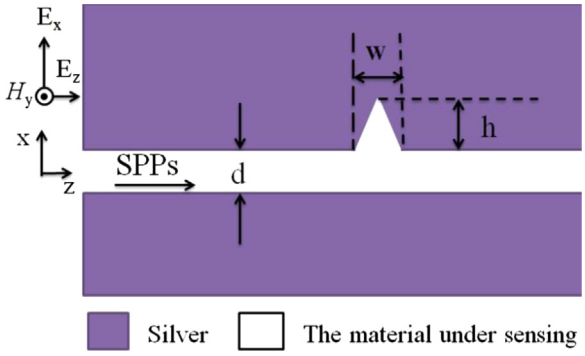

Fig. 1. Structure schematics of metal–insulator–metal (MIM) waveguide with a triangle defect, d is width of the slit, w and h are the width and the height of the defect, respectively.

MIM structure can be written as [1,9]

$$\frac{\varepsilon_i p}{\varepsilon_m \kappa} = \frac{1-\exp(kd)}{1+\exp(kd)}, \tag{1}$$

where $\kappa = (\beta_{SPPs}^2 - \varepsilon_i \kappa_0^2)^{1/2}$ and $p = (\beta_{SPPs}^2 - \varepsilon_m \kappa_0^2)^{1/2}$. β_{SPPs} is the propagation constant and $\kappa_0 = 2\pi/\lambda$ is the free-space wave vector. ε_i is the dielectric constant of the insulator. The frequency-dependent complex relative permittivity ε_m of silver is characterized by the Drude model.

$$\varepsilon_m(\omega) = \varepsilon_\infty - \frac{\omega_p^2}{\omega^2 + i\omega\gamma}, \tag{2}$$

where $\varepsilon_\infty = 3.7$, $\omega_p = 9.17$ eV, and $\gamma = 18$ meV. The refractive index of ethanol can be defined as

$$n = 1.36048 - 3.94 \times 10^{-4}(T - T_0), \tag{3}$$

where T_0 is the room temperature with a value of 20 °C and T is the ambient temperature. The definition Eq. (3) displays the linear relationship between the refractive index of ethanol and temperature. In the following finite element method (with COMSOL Multiphysics 4.3a) simulations, scatter boundary conditions are used, the fundamental TM mode of the SPPs is excited by a port on the left side of the slit. The transmission is defined to be $T = P_{out}/P_{in}$.

3. Results and discussions

Fig. 2(a) shows the transmission spectrum of the structure. The structure parameters are set to be $d = 50$ nm, $w = 50$ nm, and $h = 80$ nm, respectively. The refractive index of the material under sensing, n, is assumed to be 1, which is the refractive index of air. In Fig. 2(a), it can be seen that the transmission characteristics of the metal–insulator–metal (MIM) waveguide with a triangle defect is different from the metal–insulator–metal (MIM) waveguide with no defect (straight MIM slit waveguide), there is a dip in the transmission spectrum of the metal–insulator–metal (MIM) waveguide with a triangle defect which occurs at the free-space wavelength at nearly 580 nm with a FWHM of 52 nm. The maximum transmittance at the wavelengths longer than 686 nm is over 90%, so this structure is of a filtering function. Fig. 2(b)–(d) depicts the contour profiles of fields H_y for different wavelengths. In Fig. 2(b)–(d), the wavelengths of the SPPs are $\lambda = 490$ nm, $\lambda = 580$ nm, and $\lambda = 1000$ nm, respectively. The field distribution in Fig. 2(c) corresponds to the dip in Fig. 2(a). As can be seen in Fig. 2(c), evidently, almost no SPPs exist in the right-side of the defect, the transmission of SPPs is forbidden in this case. From the results in Fig. 2(a)–(d), we can get the conclusion that the waveguide with a single defect could generate a dip in the transmission spectrum, the dip is related to strong absorption at the defect location due to localized surface plasmon resonances, and at the dip wavelength the field enhancement is the most intense. As a sensor, we need to find reasonable structure parameters at first.

Fig. 3(a) shows the transmission spectrum of the structure with various triangle defect widths of w. Where the triangle defect height is set to be $h = 100$ nm, the slit waveguide width is set to be $d = 50$ nm and the refraction index is set to be $n = 1$. As can be seen from Fig. 3(a), the dip of the transmission spectrum exhibits blue shift as the defect width increases. Fig. 3(b) shows the dip position of the transmission spectrum versus the triangle defect width w. The triangle defect width w is set to vary from 10 nm to 600 nm, the parameters of d, h and n are set to be 50 nm, 100 nm, and 1, respectively. As shown in Fig. 3(b), the dip position shifts very significantly to the short wavelength (blue-shift) with an increase of w for $w < 40$ nm, the shift rate rapidly becomes small after $w > 40$ nm, and tends to constant value after $w > 300$ nm. Fig. 4 shows the transmission spectrum of the structure with different triangle defect heights of $h = 20$ nm, 40 nm, 50 nm, and 80 nm, the parameters of d, w and n are set to be 50 nm, 50 nm, and 1, respectively. It is found that the wavelength of the dip position exhibits red shift when h increases. But there are no dips appearance in the transmission spectrum when $h = 20$ nm. As the design of a sensor, we use the function relationship between the dip position of the transmission spectrum and the refractive index of the material under sensing, or ambient temperature. Therefore, the width of the triangle defect does not need too big, and the height of the triangle defect cannot be small.

Then we analyze the refractive index sensing characteristics of the structure. Fig. 5(a) depicts the transmission spectrum of the structure for different refractive index of 1–1.5 in steps of 0.1, the parameters of d, w and h are set to be 50 nm, 50 nm, and 80 nm, respectively. The FEM simulation results reveal that the dip position of the transmission spectrum exhibits red-shift with the increasing of the refractive index of the material under sensing. Fig. 5(b) displays the linear relationship between the dip position of the transmission spectrum and the refractive index of the material under sensing with $d = 50$ nm, $w = 50$ nm, and $h = 80$ nm. The refractive index sensitivity is defined as $d\lambda/dn$, it can be obtained 516 nm RIU^{-1}, and it possesses a higher FOM with a value of 10.32 in comparison with some numerical simulation reports [8–10,14]. According to the linear relationship between the dip position of the transmission spectrum and the refractive index n as shown in Fig. 5(b), the refractive index of the material under sensing can be obtained from being detected the dip wavelength of the transmission spectrum, this is the sensing principle of the structure as a refractive index sensor.

Next, we would like to study the influence of the structural parameters on the refraction index sensing sensitivity. Fig. 6(a) shows that the dip position of the transmission spectrum as a function of the refractive index for different defect heights of $h = 80$ nm, 160 nm, 220 nm and 300 nm, respectively. The parameters of d and w are set to be 50 nm and 50 nm, respectively. As can be seen from Fig. 6(a), the defect height can change the position of the dip wavelength markedly, while the defect heights are set to be 80 nm, 160 nm, 220 nm and 300 nm, respectively, the refractive index sensitivities are 516 nm RIU^{-1}, 986 nm RIU^{-1}, 1296 nm RIU^{-1} and 1736 nm RIU^{-1}, correspondingly; it can be obtained the FOM of 10.32, 11.20, 8.64 and 9.79, correspondingly. The calculation results indicate that the refractive index sensitivity is improved with the defect height increasing. Fig. 6(b) displays that the dip position of the transmission spectrum as a function of the refractive index for different widths of the defect with $w = 20$ nm, $w = 50$ nm and $w = 100$ nm, respectively. The

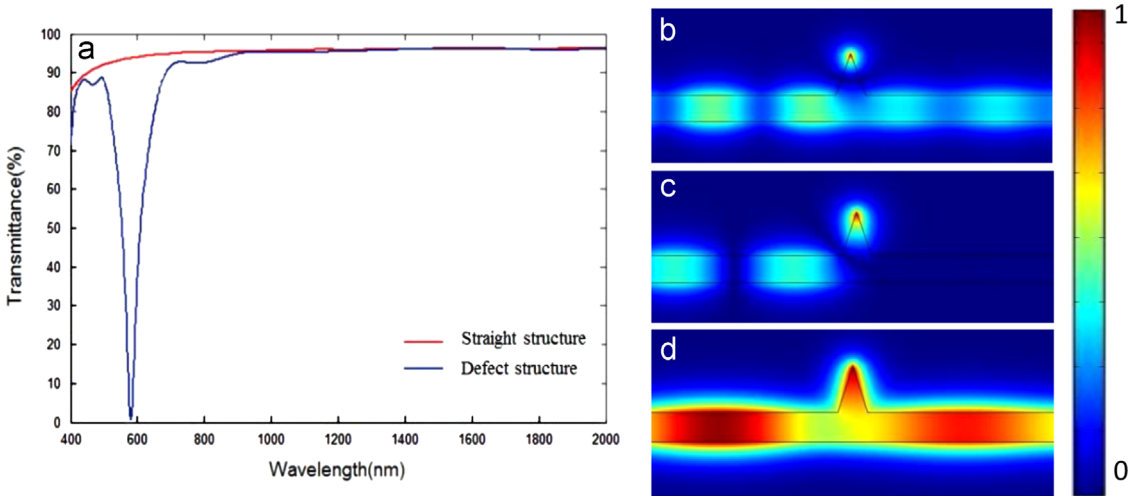

Fig. 2. (a) The transmission spectrum of the metal–insulator–metal (MIM) waveguide with a triangle defect compared with a straight MIM slit waveguide. The width of the slit is d =50 nm, the width and the height of the defect are 50 nm and 80 nm, respectively. The refractive index of the material under sensing, n, is set to be 1. The contour profiles of field H_y of the SPPs waveguide with a single defect at different wavelengths (b) λ =490 nm, (c) λ =580 nm and (d) λ =1000 nm.

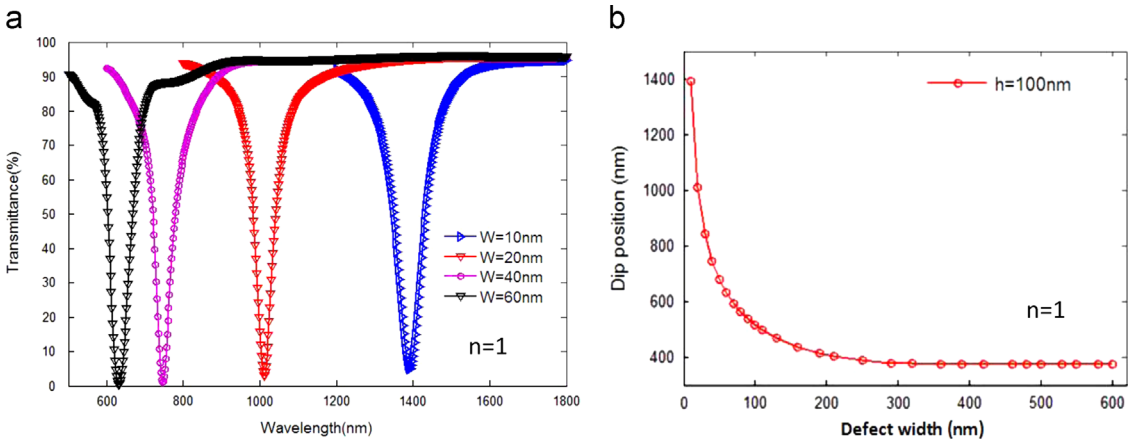

Fig. 3. (a) The transmission spectrum of the structure for different triangle defect widths w with a fixed triangle defect height of h =100 nm, the parameters of d and n are set to be 50 nm and 1, respectively. (b) The dip position of the transmission spectrum versus the defect width w.

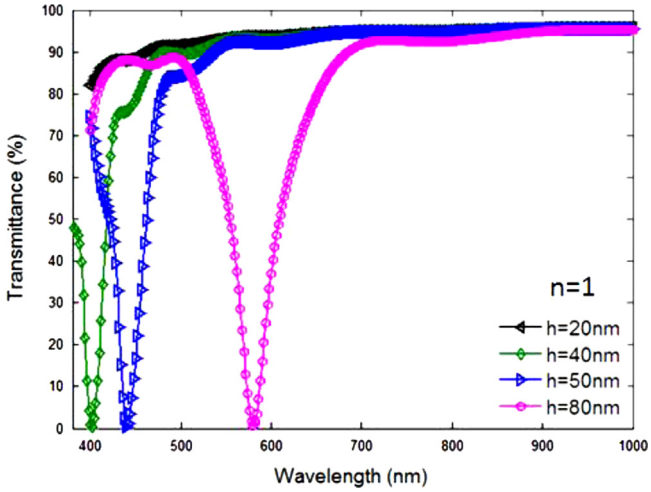

Fig. 4. The transmission spectrum of the structure for different defect heights of h, the parameters of d, w and n are set to be 50 nm, 50 nm, and 1, respectively.

parameters of d and h are set to be 50 nm and 80 nm, respectively. While w is set to be 20 nm, 50 nm and 100 nm, respectively, the refractive index sensitivity is 804 nm RIU^{-1}, 516 nm RIU^{-1}, and 368 nm RIU^{-1}, correspondingly; the FOM is 14.36, 10.32, and 7.08, respectively. The calculation results indicate that the refractive index sensitivity is lower with the width of the defect increasing. Therefore, we can improve the sensitivity of the SPPs sensor by means of increasing the height of the defect or decreasing the width of the defect. According to the above analysis, the focal point of the device, is the apex curvature of the defect. If the apexes are not so sharp, it will result in lower refractive index sensitivity.

Finally, this paper is analyzed on the temperature sensing characteristics of the structure. As a temperature sensor, we need to find a liquid with high refractive index temperature coefficient at first, then fill it into the slit and the defect, and seal the liquid at last. Here we choose ethanol, the refractive index temperature coefficient of ethanol as high as 3.94×10^{-4}, Eq. (3) displays the linear relationship between the refractive index of ethanol and temperature, while the dip position of the transmission spectrum has a linear relationship with the refractive index n of the material under sensing according to the above analysis, so the dip position of the transmission spectrum has a linear relationship with temperature. Fig. 7 shows the dip position shift with temperature changing with d =50 nm. As for temperature sensing, the sensitivity can be defined as $d\lambda/dT$, it can be obtained 0.20 nm/°C for w =50 nm, h =80 nm, 0.39 nm/°C for w =50 nm, h =160 nm,

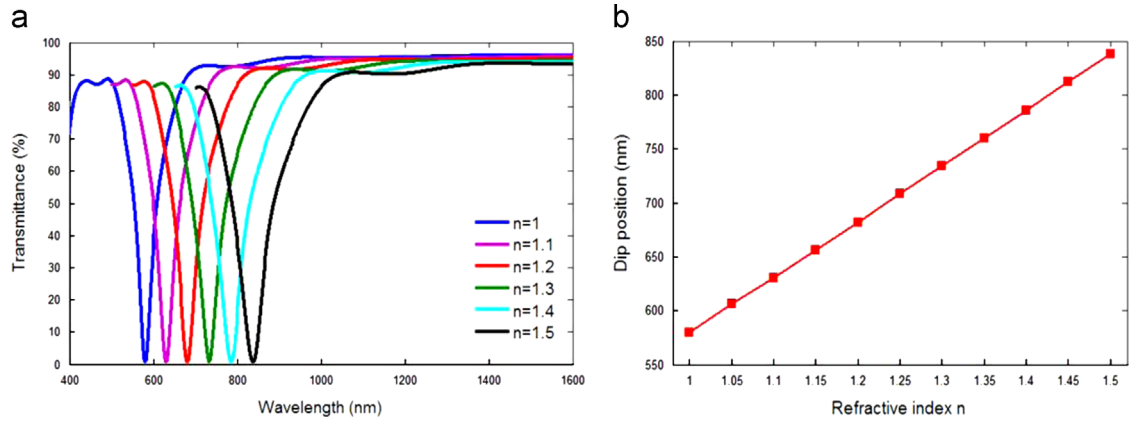

Fig. 5. (a) The transmission spectrum of the structure for different refractive index n with d =50 nm, w =50 nm, and h =80 nm. (b) The dip position of the transmission spectrum versus the refractive index n of the material under sensing.

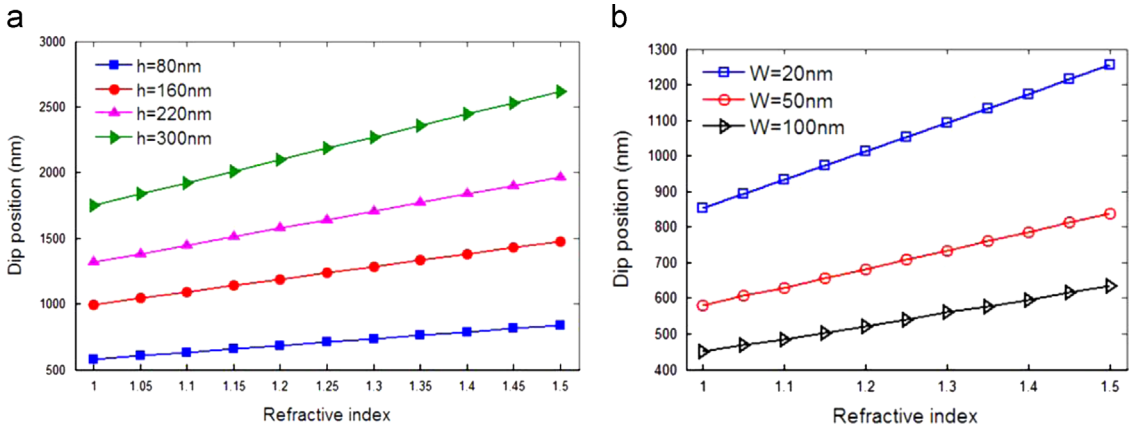

Fig. 6. (a) The dip position of the transmission spectrum versus the refractive index of the material under sensing with different defect heights and given d =50 nm and w =50 nm. (b) The dip position of the transmission spectrum versus the refractive index of the material under sensing with different defect widths and given d =50 nm and h =80 nm.

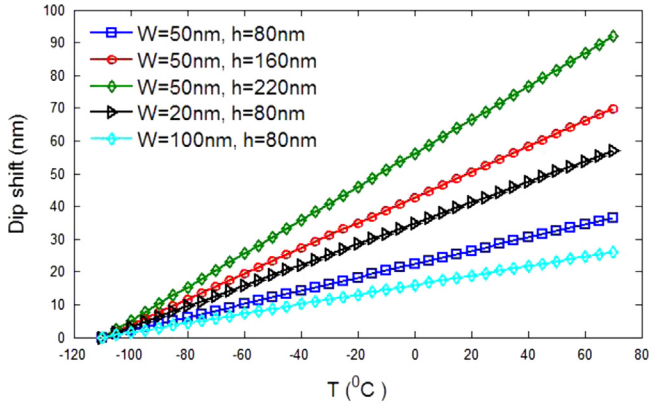

Fig. 7. The dip shift versus the temperature with different w and h, the width of the slit is d =50 nm.

0.51 nm/°C for w =50 nm, h =220 nm, 0.32 nm/°C for w =20 nm, h =80 nm, and 0.15 nm/°C for w =100 nm, h =80 nm, respectively. Because the melting point of ethanol is −114.3 °C, and the boiling point is 78 °C, so the device which filled with ethanol is suitable for low temperature sensing.

4. Conclusion

In conclusion, we have proposed a metal–insulator–metal (MIM) waveguide with a triangle defect for refractive index sensing and temperature sensing. The sensing characteristics of the structure have been simulated by 2D finite element method. The simulation results show that the dip position of the transmission spectrum has a linear relationship with the refraction index of the material under sensing or ambient temperature. When the apex curvature of the defect is very sharp, this structure not only has higher sensing sensitivity but also can obtain higher figure of merit (FOM). Furthermore, the miniaturization and simple structure of the device make it easy to integrate into chips. The proposed structure has extensive potential in nanoscale industrial sensing.

Acknowledgments

The work was supported by the National Natural Science Foundation of China (61275201), the Program for New Century Excellent Talents in University of Ministry of Education of China (Grant no. NCET-10-0261), the Fund of State Key Laboratory of Information Photonics and Optical Communications (Beijing University of Posts and Telecommunications), PR China, the Fundamental Research Funds for the Central Universities of Ministry of Education of China (Grant no. 2011RC0402), the Research Fund for the Doctoral Program of Higher Education of China (Grant no. 20100005110013), and the Opened Fund of the State Key Laboratory on Integrated Optoelectronics, Institute of Semiconductors, Chinese Academy of Sciences.

References

[1] Tongbiao Wang, Xiewen Wen, Chengping Yin, Opt. Express 17 (2009) 24096.
[2] Yi Song, Min Yan, Qing Yang, Limin Tong, Min Qiu, Opt. Commun. 284 (2011) 480.
[3] Qiang Li, Yi Song, Gan Zhou, Yikai Su, Min Qiu, Opt. Lett. 35 (2010) 3153.
[4] Min Yan, Lars Thylen, Min Qiu, Opt. Express 19 (2011) 3818.
[5] Kristof Lodewijks, Jef Ryken, Willem Van Roy, Gustaaf Borghs, Plasmonics 8 (2013) 1379.
[6] Vasily V. Temnov, Gaspar Armelles, Ulrike Woggon, Dmitry Guzatov, Nat. Photonics 4 (2012) 107.
[7] Diana Martín-Becerra, Juan B. González-Díaz, Vasily V. Temnov, Appl. Phys. Lett. 97 (2010) 183114.
[8] Fei Fan, Sai Chen, Xianghui Wang, Shengjiang Chang, Opt. Express 21 (2013) 8614.
[9] Alireza Dolatabady, Nosrat Granpayeh, Vahid Foroughi Nezhad, Opt. Commun. 300 (2013) 265.
[10] Vladimir E. Bochenkov, Maj Frederiksen, Duncan S. Sutherland, Opt. Express 21 (2013) 14763.
[11] Jian Zhu, Jianjun Li, Junwu Zhao, J. Nanopart. Res. 15 (2013) 1721.
[12] Soren Raza, Giuseppe Toscano, Antti-Pekka Jauho, Plasmonics 8 (2013) 193.
[13] Marek Piliarik, Hana Šípová, Pavel Kvasnička, Opt. Express 20 (2012) 673.
[14] J.J. Mock, R.T. Hill, A. Degiron, S. Zauscher, Nano Lett. 8 (2008) 2245.
[15] E.M. Larsson, J. Alegret, M. Käll, D.S. Sutherland, Nano Lett. 7 (2007) 1256.
[16] Jia Hu Zhu, Xu Guang Huang, Jin Tao, Xiao Ping Jin, Opt. Commun. 285 (2012) 3242.
[17] Antoine Lesuffleur, Hyungsoon Im, Nathan C. Lindquist, Appl. Phys. Lett. 90 (2007) 243110.
[18] Benjamin Gallinet, Martin Olivier J.F., ACS Nano 7 (2013) 6978.
[19] Mengxin Ren, Chongpei Pan, Qunqing Li, Wei Cai, Opt. Lett. 38 (2013) 3133.
[20] Feng Hao, Peter Nordlander, Yannick Sonnefraud, ACS Nano 3 (2013) 643.
[21] Yuan Hsing Fu, Jing Bo Zhang, Ye Feng Yu, ACS Nano 6 (2013) 5130.
[22] Jianhong Zhou, Xiping Xu, Wenbo Han, Opt. Express 21 (2013) 12159.
[23] Tun Cao, Lei Zhang, Opt. Express 21 (2013) 19228.
[24] Xiubao Kang, Haidong Li, Jun Ding, Opt. Lett. 38 (2013) 715.
[25] Yang Shen, Jianhua Zhou, Tianran Liu, Yuting Tao, Ruibin Jiang, Nat. Commun. 4 (2013) 2381.
[26] K.M. Mayer, J.H. Hafner, Chem. Rev. 111 (2011) 3828.
[27] A.G. Brolo, Nat. Photonics 6 (2012) 709.